Comparison of measured and computed radial trajectories of plasma focus devices UMDPF1 and UMDPF0

8 authors, including:

Ling Hong Lim
4 PUBLICATIONS   0 CITATIONS

SEE PROFILE

Yap Seong Ling
University of Malaya
98 PUBLICATIONS   233 CITATIONS

SEE PROFILE

Poh Hun Seng
University of Malaya
1 PUBLICATION   0 CITATIONS

SEE PROFILE

Sing Lee
INTI International University
393 PUBLICATIONS   3,529 CITATIONS

SEE PROFILE

Comparison of measured and computed radial trajectories of plasma focus devices UMDPF1 and UMDPF0

L. H. Lim, S. L. Yap, L. K. Lim, M. C. Lee, H. S. Poh, J. Ma, S. S. Yap, and S. Lee

Articles you may be interested in

External circuit integration with electromagnetic particle in cell modeling of plasma focus devices
Phys. Plasmas **22**, 033514 (2015); 10.1063/1.4916046

Characterization of the axial plasma shock in a table top plasma focus after the pinch and its possible application to testing materials for fusion reactors
Phys. Plasmas **21**, 122703 (2014); 10.1063/1.4903471

Modelling of the internal dynamics and density in a tens of joules plasma focus device
Phys. Plasmas **19**, 012703 (2012); 10.1063/1.3672005

Temporal and spatial study of neon ion emission from a plasma focus device
Phys. Plasmas **18**, 033101 (2011); 10.1063/1.3560884

Computing plasma focus pinch current from total current measurement
Appl. Phys. Lett. **92**, 111501 (2008); 10.1063/1.2899632

Comparison of measured and computed radial trajectories of plasma focus devices UMDPF1 and UMDPF0

L. H. Lim,[1] S. L. Yap,[1,a)] L. K. Lim,[1] M. C. Lee,[1] H. S. Poh,[1] J. Ma,[1] S. S. Yap,[2,3] and S. Lee[1,4,5]

[1]*Plasma Technology Research Centre, Department of Physics, Faculty of Science, University of Malaya, 50603 Kuala Lumpur, Malaysia*
[2]*UMPEDAC, University of Malaya, 50603 Kuala Lumpur, Malaysia*
[3]*Faculty of Engineering, Multimedia University, Cyberjaya, 63100 Selangor, Malaysia*
[4]*INTI International University, 71800 Nilai, Malaysia*
[5]*Institute for Plasma Focus Studies, 32 Oakpark Drive, Chadstone 3148, Australia*

In published literature, there has been scant data on radial trajectory of the plasma focus and no comparison of computed with measured radial trajectory. This paper provides the first such comparative study. We compute the trajectories of the inward-moving radial shock and magnetic piston of UMDPF1 plasma focus and compare these with measured data taken from a streak photograph. The comparison shows agreement with the measured radial trajectory in terms of average speeds and general shape of trajectory. This paper also presents the measured trajectory of the radially compressing piston in another machine, the UMDPF0 plasma focus, confirming that the computed radial trajectory also shows similar general agreement. Features of divergence between the computed and measured trajectories, towards the end of the radial compression, are discussed. From the measured radial trajectories, an inference is made that the neutron yield mechanism could not be thermonuclear. A second inference is made regarding the speeds of axial post-pinch shocks, which are recently considered as a useful tool for damage testing of fusion-related wall materials. © 2015 AIP Publishing LLC. [http://dx.doi.org/10.1063/1.4929856]

I. INTRODUCTION

Experimental studies of the dense plasma focus have recently uncovered the complexity of the pinched plasma[1] with the components of current flowing in the dense column and the surrounding. A complete description of the plasma behaviour has yet to be revealed, but the broad range of emissions particularly neutron and x-ray emissions has been extensively studied and characterised.[1–7] Numerical descriptions of the plasma dynamic based on MHD model[8] assumed a fully ionised two fluid system, the high temperature achieved during the radial compression was contributed by adiabatic compression, viscous heating, and joule heating. Thermal neutron emission could be estimated from the dense column and was found lower than experimentally observed. Non-thermal neutron emissions are often related to the sausage and kink instabilities during the pinch. Production of the high energy particle due to MHD instabilities in Z-pinch plasma was investigated by using a three-dimensional relativistic and fully electromagnetic particle-in-cell code.[9] Plasma dynamics prior to the formation of pinch have not been discussed. Two dimensional electromechanical model of the plasma focus proposed by Gratton and Vargas has shown that the time evolution of the axisymmetric current layer can be solved exactly by analytic methods. The solution suggested that large variety of self-similar profiles were possible and these sheaths focused onto a small region producing point like emissions in certain directions.[10] The

Gratton-Vargass two-dimensional model was extended to incorporate the circuit resistance and enabled the construction of a special orthogonal coordinate system in which the plasma flow problem can be simplified and formulated.[11] Thus, a global parametric optimization of the Mather-type plasma focus based on a numerical formula for its dynamic inductance, determined by fitting inductance data calculated from thousands of automated computations, was proposed.[12] These models often start with rigorous theoretical basis thus the understanding of the dynamics and properties of the plasma are limited strictly with the predefined conditions.

On the other hand, the plasma focus discharge could be simulated by considering its equivalent discharge circuit[13] using estimated resistance and inductance within the tube. An equivalent circuit model simulates only the electrical characteristics, while the component corresponds to the highly dynamical plasma could only be fitted based on experimentally measured data. Lee model was established and improved based on empirical results.[14–20] The code uses the snow-plow model[20] in the axial phase, the slug model[19] with thermodynamics in the early radial phase and a radiation-coupled compression[15,16,18] in the pinch phase; all the phases being rigorously circuit-coupled so as to be energy- and charge-consistent besides being momentum- and mass-consistent.

The simple treatment of the axial and early radial phases has produced several important insights into general plasma focus behaviour such as an optimum static inductance[17] and current and neutron scaling and saturation.[14] The radiation-coupled equation of motion used in the pinch phase has

---

a)Electronic mail: yapsl@um.edu.my

postulated the radiative-collapse when the pinch current exceeds Pease-Braginskii current.[18] This has enabled pioneering work on the investigation of radiative-collapse in the plasma focus using the PF1000.

Many aspects of the code, such as machine optimisation, neutron and soft x-ray yields, and scaling, have been compared or related to laboratory measurements.[21–29] In terms of dynamics specifically, comparison of the computed axial phase trajectory of the plasma focus with measurements had been made in several plasma focus devices.[29–35] However, there have not been published any such comparative studies of trajectory of the radial phase, as evidenced by a literature search including, for example, two comprehensive review papers.[36,37]

In a recent internal review of research results from our laboratory, we found valuable data obtained from a streak photograph of the plasma focus radial compression, analysed, and recorded in the 1989 Ph.D. thesis by Kwek.[38] We also found a sequence of high speed photographs imaging the radial phase of the plasma focus, analysed and recorded in a 1972 thesis by Chen.[39] The two plasma focus machines are the UMDPF0 (Ref. [39]) and the UMDPF1,[38] both are Mather-type.[40] Moreover, corresponding to each of these two shots a current waveform was also recorded. In this paper, for each shot we fit the computed current waveform generated by the Lee model code to the measured current waveform, thus obtaining the model parameters which enable us to fully configure the code in each case. The resulting radial trajectories calculated for the two machines are then compared with the measured data. In this paper, we present the comparison of the measured radial dynamics of UMDPF1 and UMDPF0 with Lee model code computations.

II. BASIS OF THE NUMERICAL EXPERIMENT

In the Lee model code, five phases are considered including the axial phase (based on snow-plow model[20]), radial inward shock phase, radial reflected shock phase, slow compression phase, and expanded column axial phase. The radial phases include both the radial inward shock phase and the radial reflected shock phase that incorporate the dynamics, thermodynamics, and electrodynamics of the system. The radial inward shock phase is characterised by a slug model[19] with a shockwave at the front of a layer of plasma (slug) and a magnetic piston (at the position of the current sheath) at the rear of the slug, propelling the slug towards the axis of the system. When the shockwave coalesce on-axis, a reflected shock is formed. Four equations are used to describe the radial inward shock phase and the radial reflected shock phase.[15,16] The four equations include equations for radial shock front speed, dr_s/dt, axial elongation speed, dz_f/dt, radial piston speed, dr_p/dt, and rate of change of electric current, dI/dt; where r_s is the position of the inward moving shock front, r_p is the magnetic piston, z_f is the length of slug, and I is the driving current (refer Fig. [1]).

The radial shock front speed, dr_s/dt, derived from shock theory[15] with an assumption of uniform pressure from the shock front to the current sheet is given as
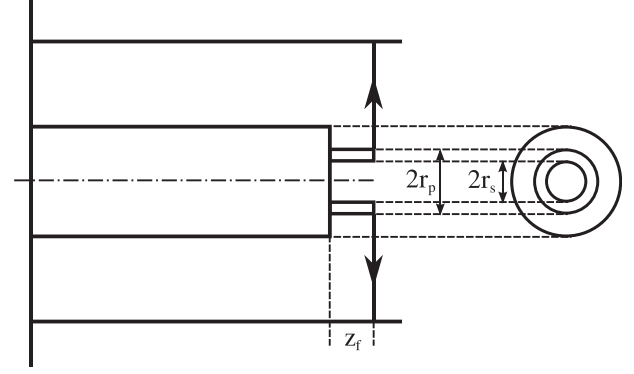

FIG. 1. Radial phase diagram, where r_s is the position of the inward moving shock front, r_p is the magnetic piston position, and z_f is the length of the plasma slug.

$$\frac{dr_s}{dt} = -\left[\frac{\mu(\gamma+1)}{\rho_0}\right]^{1/2} \frac{f_{cr}}{\sqrt{f_{mr}}} \frac{I}{4\pi r_p},$$

where μ is the permeability, γ is the specific heat ratio of the plasma, ρ_0 is the ambient density, f_{cr} is the fraction of current flowing in current sheet, and f_{mr} is the effective mass fraction swept into the radial slug. Both f_{cr} and f_{mr} are known as the radial model parameters. The axial elongation speed of current speed is taken as

$$\frac{dz_f}{dt} = -\left(\frac{2}{\gamma+1}\right)\frac{dr_s}{dt}.$$

In the radial piston speed equation, the assumption of adiabatic relationship and the use of slug model give us the radial piston speed as

$$\frac{dr_p}{dt} = \frac{\frac{2}{\gamma+1}\frac{r_s}{r_p}\frac{dr_s}{dt} - \frac{r_p}{\gamma I}\left(1-\frac{r_s^2}{r_p^2}\right)\frac{dI}{dt} - \frac{r_p}{z_f}\left(1-\frac{r_s^2}{r_p^2}\right)\frac{dz_f}{dt}}{\frac{\gamma-1}{\gamma} + \frac{1}{\gamma}\frac{r_s^2}{r_p^2}}.$$

The electric current is given by

$$\frac{dI}{dt} = \frac{V_0 - \frac{\int I dt}{C_0} - r_0 I - f_c \frac{\mu}{2\pi}\left(\ln\frac{b}{r_p}\right)I\frac{dz_f}{dt} + f_c \frac{\mu}{2\pi}\frac{z_f}{r_p}I\frac{dr_p}{dt}}{L_0 + f_c \frac{\mu}{2\pi}(\ln c)z_0 + f_c \frac{\mu}{2\pi}\left(\ln\frac{b}{r_p}\right)z_f},$$

where V_0 is the charging voltage, L_0 is the static inductance, C_0 is the bank capacitance, r_0 is the short-circuited bank resistance, and z_0 is the anode length. We obtain the four variables r_s, r_p, z_f, and I by numerically integrating the four coupled differential equations. The integration is done step-by-step in time using Microsoft Excel Visual Basic platform. The specific heat ratio of the plasma is evaluated at each time point using shock theory to obtain the plasma temperature and corona model to obtain the dominant ionisation fractions.[15,16]

The reflected shock phase starts when the radial inward shock front reaches the axis. The equations in the radial reflected shock phase are the reflected shock
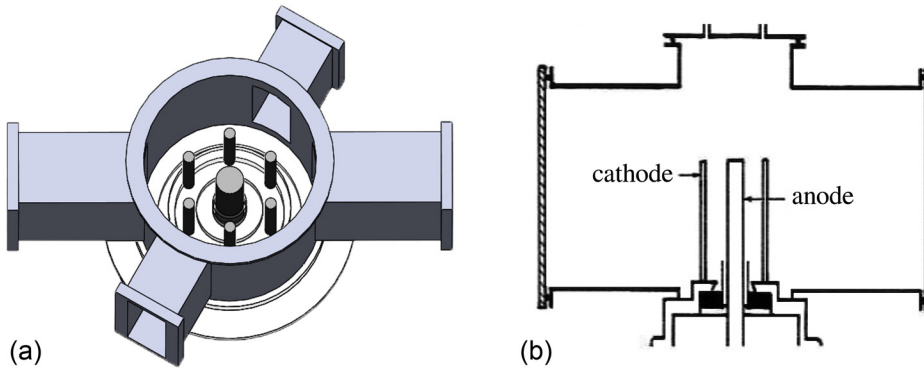
FIG. 2. UMDPF1—a copper anode surrounded by six cathode rods, and housed in a vacuum chamber with viewports.

speed, $dr_r/dt = -0.3(dr_s/dt)$, elongation speed, $dz_f/dt = -(2/(\gamma+1))(dr_s/dt)$, where dr_s/dt is the radial inward on-axis shock speed. The piston speed is given as

$$\frac{dr_p}{dt} = \frac{-\dfrac{r_p}{\gamma I}\left(1-\dfrac{r_s^2}{r_p^2}\right)\dfrac{dI}{dt} - \dfrac{r_p}{z_f}\left(1-\dfrac{r_s^2}{r_p^2}\right)\dfrac{dz_f}{dt}}{\dfrac{\gamma-1}{\gamma} + \dfrac{1}{\gamma}\dfrac{r_s^2}{r_p^2}}$$

and circuit equation is the same as in radial inward shock phase. The phase ends when the radially out-going reflected shock front meets the radially incoming magnetic piston. Then the pinch phase starts.

The pinch phase is treated with a radiation-coupled piston equation which computes the position of the piston with the help of a Bennett-type equation[41] which determines the temperature of the column, and radiation equations which estimate the Bremsstrahlung, recombination, and line radiations. Joule heating is also incorporated into the piston equation. The computation is terminated by using the transit time of small disturbance speeds across the column as the termination criterion. In this manner, the piston trajectory is computed from the start to the end of the radial pinch phase. It is important to note that the model incorporates plasma self-absorption of radiation[42] to more correctly estimate the radiation effect on the piston motion. The model also incorporates the all-important effect of "communication delay" between the shock-front and magnetic piston.[19] Without incorporating this "Potter-effect" the radial speeds could be over-estimated by a factor as much as two.[43]

III. PROCEDURE FOR NUMERICAL EXPERIMENT

The code is configured as the UMDPF0 or UMDPF1, as the case may be; using the relevant bank parameters (L_0, C_0 and r_0), tube parameters (z_0, a, the length and radius of the inner electrode and b, the radius of the outer electrode), and operational parameters (V_0, P_0 the charging voltage and operating pressure; and type of gas is also specified). Trial model parameters are used and the computed current waveform is fitted to the measured current waveform by adjusting the model parameters. First, the axial phase part of the current waveform is fitted by adjusting the axial phase model parameters f_m and f_c until the computed axial phase part of the current waveform up to the current dip is correctly fitted to the corresponding part of the measured current waveform. Then the current dip, which corresponds to the radial phase, is fitted by varying f_{mr} and f_{cr}. During the fitting process, discrepancy in the shape of the computed current rise profile with that of the measured rise profile may require the value of L_0 (as provided by source thesis) to be adjusted to fit the computed profile to the measured. Typically, the value of L_0 provided by the experimenter is a nominal one estimated, for example, from short-circuited discharge. This may not be the full static inductance L_0 which should include also the inductance of the plasma focus collector plates. The length z_0 of the anode is also treated as a nominal value since there is a glass-insulator surrounded section. Typically, the effective length is also found during the fitting.

IV. UMDPF1 AND RESULTS

The UMDPF1 was a Mather-type plasma focus with the length of 16 cm of copper anode in the centre surrounded by six equally spaced copper rods of length 16 cm and placed in a circle of diameter 8.5 cm so as to form the cathode (the setup is depicted in Fig. 2). The system was housed in a vacuum chamber with viewports that enable high speed photography for time-resolved imaging studies. Table I gives the bank, tube, and operational parameters[38] with our initial trial model parameters. The single asterisk indicates parameters which needed to be adjusted during the fitting in order to get the optimum fit as shown in Fig. 3.

TABLE I. Operational and trial model parameters for UMDPF1 operated in deuterium. E_0 is the energy of the bank, C_0 is the bank capacitance, V_0 is the charging voltage, r_0 is the short-circuited resistance, a and z_0 are the anode radius and length, respectively, b is the outer electrode radius, L_0 is the static inductance, P_0 is the operating pressure, and f_m, f_c, f_{mr}, and f_{cr} are the four trial model parameters.

$z_0{}^{\text{a}}$ (cm)	E_0 (kJ)	C_0 (μF)	V_0 (kV)	$r_0{}^{\text{a}}$ (mΩ)	a (cm)	b (cm)	$L_0{}^{\text{a}}$ (nH)	P_0 (Torr)	$f_m{}^{\text{b}}$	$f_c{}^{\text{b}}$	$f_{mr}{}^{\text{b}}$	$f_{cr}{}^{\text{b}}$
16	6.1	62	14	3.5	1.25	4.25	52	6.75	0.1	0.7	0.2	0.7

[a]Nominal values, collected from the source thesis[38] which were necessary to be changed to get a good fit.
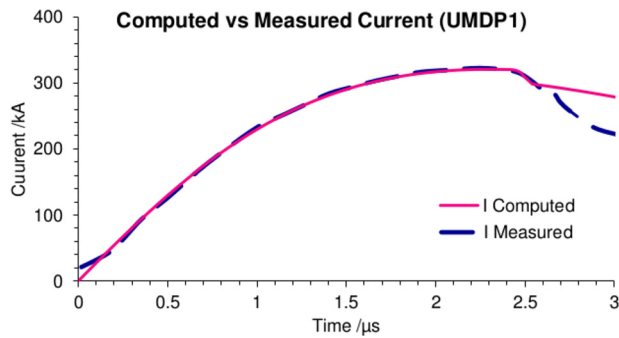[b]Initial trial values of model parameters.

FIG. 3. Measured and computed current waveform for UMDPF1.

FIG. 4. This streak photo of plasma self-light was taken on a Hadland image converter with streak module; and the time scale was checked from a monitoring waveform.[38]

The optimum fit of the model current trace to the experimental current waveform is shown in Fig. 3. The fitted values are given in Table II.

Once the computed current trace is fitted to the experimental current trace, the model code is configured for the machine, UMDPF1. The model code then generates outputs of the dynamics, plasma properties and yields of neutrons, bremsstrahlung, and line radiation with the selected input experimental parameters. A streak photograph of the self-luminosity of the radial phase of UMDPF1 corresponding to the current waveform of Fig. 3 is shown in Fig. 4. The slit through which the streak was taken had a width of 1 mm, was oriented perpendicular to the axis of symmetry (z) of the focus, and was placed 3 mm from the anode end. The slit was electronically streaked in time in the z-direction. This arrangement placed the streaked image near the center of the final pinch length and ensured that the radial dynamics (r-direction) of the pinch column at axial position of $z = 3$ mm was imaged in the last 10 mm of radial motion. The shaded zone in Fig. 5 indicates the region seen by streak camera through the slit. This $r - t$ streak image is compared with the computed radial phase (Fig. 6) with the code configured as the UMDPF1. We first compare the gross dynamics shown in Fig. 6.

The computed and measured average speeds for the inward shock are 13.7 cm/μs and 13.9 cm/μs, respectively. The computed and measured average inward piston speed which are measured from the start (time = 0) to the inflection point of each trajectory (just before $t = 100$ ns) are found to be 11.1 cm/μs and 11.9 cm/μs, respectively.

Looking into more details of the radial dynamics, the computed inward shock speed agrees well with the measured down to 2 mm from the axis of symmetry. Closer to the axis than 2 mm the measured shock speed can be seen (Fig. 6) to increase significantly to more than 30 cm/μs as the radial inward shock goes on-axis, whilst the computed does not go above 25 cm/μs. The computed inward piston speed agrees well with the measured down to almost 3 mm. Then, the piston trajectory reaches an inflection point, greatly slowing
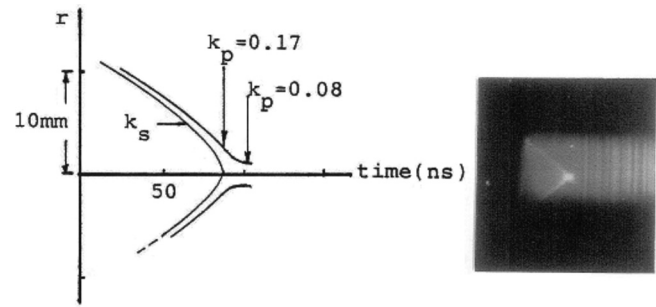
down 5 ns before the computed inward shock goes on-axis. The measured piston trajectory (luminosity rear, see Fig. 4 in correlation with Fig. 6) continues inwards even after the measured radial shock trajectory (luminous front) goes on-axis. The measured piston trajectory reaches its slowing down inflection point 10 ns after the measured radial shock front goes on-axis. Moreover, the slowing down inflection point for the computed trajectory occurs at 3 mm radius compared to the corresponding measured value of 1.5 mm. Then, the computed piston trajectory continues going towards the axis for another 50 ns attaining a minimum radius of 1.8 mm at the end of the pinch. The measured minimum radius is 1.1 mm occurring less than 10 ns after the slowing down inflection point.

In summary, there is good agreement for the dynamics of the compressing slug (both luminosity front and rear) for 90% of the compression. In the last few ns and mm, the measured radial inward shock goes on-axis significantly faster than the computed radial inward shock.

The computed piston trajectory deviates quite dramatically from the measured piston trajectory as the radial distances from the axis goes below 3 mm. The measured pinch reaches a smaller radius of 1.1 mm (radius ratio = minimum pinch radius/anode radius of 0.09) within 15 ns of the measured inward shock going on-axis. The computed piston trajectory slows down a few ns earlier, and then goes in for another 50 ns to a minimum radius of 1.8 mm (radius ratio of 0.14). These differences of the computed trajectory from the measured during the final pinch process indicate limitations of the model code and also suggest that there are mechanisms which are not as yet incorporate into the code. This is discussed further in the section VI of this paper.

V. UMDPF0 AND RESULTS

As part of the necessary exploratory experimentation, the pioneering (first installed in the early Seventies) UMDPF0 did not have the usual coaxial metallic cathode. Instead, it used a pyrex glass tube surrounding and housing

TABLE II. Operational and fitted parameters for UMDPF1 operated in deuterium.

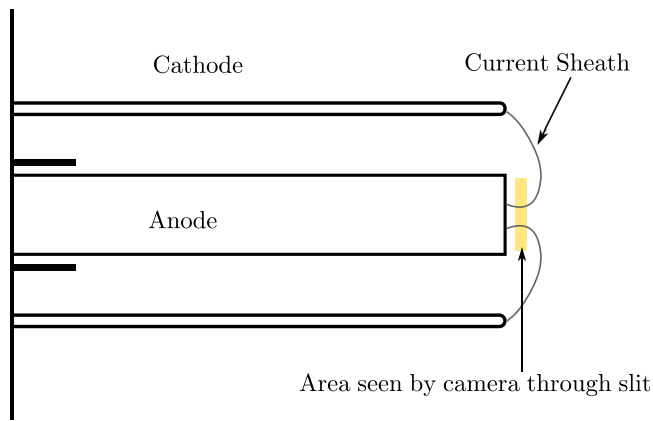| z_0 (cm)	E_0 (kJ)	C_0 (μF)	V_0 (kV)	r_0 (mΩ)	a (cm)	b (cm)	L_0 (nH)	P_0 (Torr)	f_m	f_c	f_{mr}	f_{cr}
13.9	6.1	62	14	3.2	1.25	4.25	51	6.85	0.0835	0.7	0.5	0.7

FIG. 5. The slit of the streak camera is arranged to image the radial dynamics of the pinch column. The region seen by the streak camera is indicated in the shaded zone.
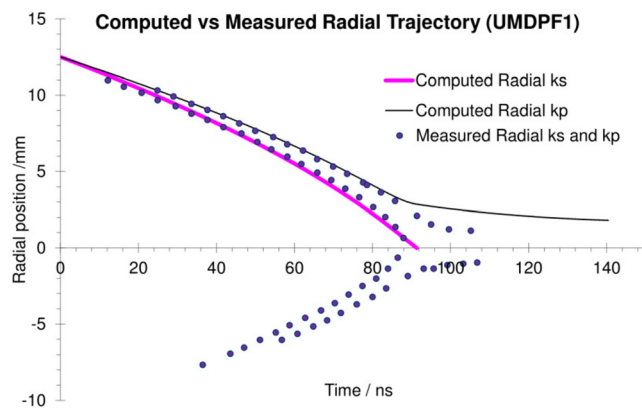

FIG. 6. Comparing computed and measured radial inward shock trajectory, k_s, and piston trajectory, k_p. The measured trajectory (digitised from Fig. 4) shows reasonable symmetry of top half and bottom half indicating good axi-symmetric for the measured radial compression. So we compare only the top half. The upper dots show the trajectory of the magnetic piston (i.e., rear of the slug), the lower dots show the trajectory of the radial inward shock (i.e., front of slug).

the copper anode to delineate the current return path. The current flows from the anode, bridges the annular space through the plasma current sheath, and returns via the layer of plasma next to the pyrex tube, to the cathode plate at the base of the pyrex tube as shown in Fig. 7. This arrangement also facilitated optical access for imaging studies for the

whole tube; using a high speed image-converter framing camera.

The bank, tube, operational and trial model parameters for this experiment are recorded in Table III. We found that L_0 had to be considered as a nominal value (it was measured from the short-circuited bank and hence did not include the inductance of the plasma focus head) which had to be varied to a correct value (see Table IV), otherwise the rising and topping part of the current waveform from 100 to 290 kA (which is crucial to the fitting process) could not be fitted. Two other parameters r_0 and z_0 also were slightly adjusted to improve the fit, but their contributions to the fit are secondary to that of L_0 for this case.

Result of the fitting is shown in Fig. 8. To simplify the fitting, the values of f_c and f_{cr} are kept as 0.7 when possible (in accordance with experimental experience) enabling a simpler fitting procedure. During the fitting it was found impossible to obtain a good fit to the rising and topping part of the current waveform without changing the value of L_0 from the nominal value (estimated from short-circuited discharge) recorded in the source thesis[39] of 58 nH. The value of L_0 was varied in steps whilst the fit was checked. Eventually, the value of 87 nH was adopted to enable a good fit. It was also necessary to make small changes to z_0 and r_0 to optimise the fitting.

We note that the measured current waveform has a humped feature that cannot be fitted. This discrepancy hump is observed for the first 0.5 μs of the computed current waveform. It is likely due to a combination of imperfect switching and the way the electrical noise of switching had affected the recording of the waveform in a poorly shielded setup. The discrepancy area of this hump is estimated as less than 3% of the total area of the current-time waveform from start of current to the end of the axial phase, this end being indicated in Fig. 7 by the start of the current dip at around $t = 1.7$ μs. Hence, we feel justified to ignore this hump and consider that the fit of computed current waveform from $t = 0.5$ μs (when $I = 100$ kA) to $t = 1.7$ μs (when $I = 290$ kA) to the measured current waveform is reasonable. Also the current dip is reasonably fitted in slope; although the computed depth of current dip falls a little short of the measured bottom of the dip. This is likely due to the UMDPF0 exhibiting post-pinch anomalous resistance features due to its relatively high (near 100 nH) L_0.[44,45] This point will be discussed further in Section VI of this paper.

(a)

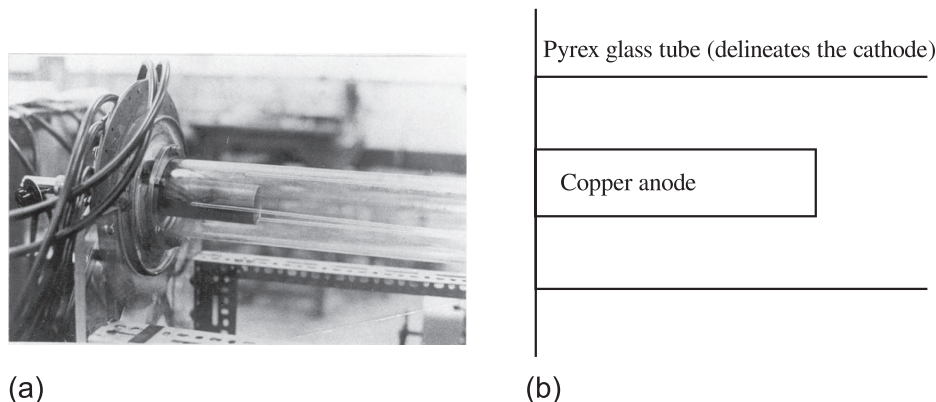Pyrex glass tube (delineates the cathode)

Copper anode

(b)

FIG. 7. UMDPF0 layout showing the copper anode in the glass tube housing: This early plasma focus did not have the usual outer coaxial metallic cathode. The pyrex glass tube delineates the current return path. The current creates its own return path along the inner surface of the glass tube.

TABLE III. Operational and trial models parameters for UMDPF0 operated in deuterium. E_0 is the energy of the bank, C_0 is the bank capacitance, V_0 is the charging voltage, r_0 is the short-circuited resistance, z_0 and a are the anode length and radius, respectively, b is the outer electrode radius, L_0 is the static inductance, P_0 is the operating pressure, and $f_m, f_c, f_{mr},$ and f_{cr} are the four trial model parameters we started with.

z_0[a] (cm)	E_0 (kJ)	C_0 (μF)	V_0 (kV)	r_0[a] (mΩ)	a (cm)	b (cm)	L_0[a] (nH)	P_0 (Torr)	f_m[b]	f_c[b]	f_{mr}[b]	f_{cr}[b]
10	6.2	31	20	4.5	2.5	4.1	58	0.3	0.1	0.7	0.2	0.7

[a]Nominal values, collected from the source thesis[39] which were found necessary to be changed to get a good fit (z_0 is varied only slightly).
[b]Initial trial values of model parameters. The fitted values are given in Table IV.

TABLE IV. Operational and fitted parameters for UMDPF0 operated in deuterium.

z_0 (cm)	E_0 (kJ)	C_0 (μF)	V_0 (kV)	r_0 (mΩ)	a (cm)	b (cm)	L_0 (nH)	P_0 (Torr)	f_m	f_c	f_{mr}	f_{cr}
11	6.2	31	20	5	2.5	4.1	87	0.3	0.375	0.7	0.85	0.7

From the fitting, the correct (fitted) configuration of UMDPF0 focus was found and recorded in Table IV.

Once the computed current waveform is correctly fitted to the measured current waveform of the UMDPF0, the Model code is deemed to be correctly configured as the UMDPF0; and the output results of the code are expected to realistically portray the actual plasma focus in terms of axial and radial dynamics, plasma properties, and radiation properties. The data on radial trajectory were taken from one series of framing photographs of self-luminosity using a Hadland intensified camera in framing mode with eight frames in one shot at time intervals set at nominal 100 ns but varied and determined by monitoring pulses. These framing photographs were taken in the same shot as the measured current waveform analysed in Fig. 8. We take the boundary of luminosity as the position of the current sheath forming the magnetic piston. We estimate the time error and position error to be, respectively, ±10 ns and ±2 mm. The relatively large errors are due to the exposure time estimated as less than 20 ns, the small size of each exposed image, and the high speeds of the pinch boundaries being recorded. The computed radial trajectory and measured trajectory of the magnetic piston are shown in Fig. 9. The comparison shows several features of agreement. The computed average speed of the magnetic piston from radial position of 25 mm to 6 mm is 19 cm/μs. The measured average speed from 25 mm to 4 mm is 21 cm/μs. The peak radial speeds of both the computed and measured trajectories are just under 25 cm/μs.
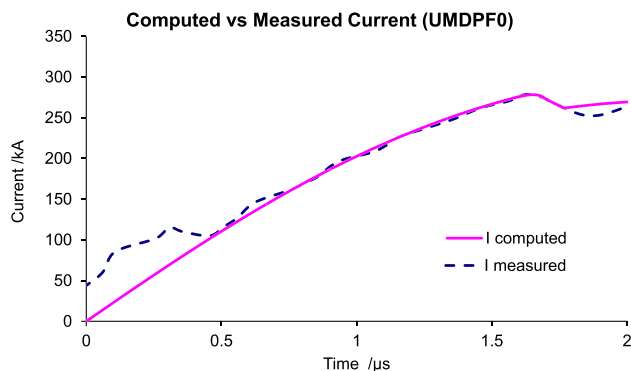
The computed radial trajectory has an inflection point at 6 mm at time of 120 ns from start of radial phase. This inflection point of the magnetic piston trajectory indicates the time when the inward radial shock goes on-axis. The corresponding point on the measured trajectory is 4 mm at time 120 ns. The computed trajectory then continues inwards to reach a minimum pinch radius of 3.5 mm at 180 ns. The corresponding part of the measured trajectory goes in to a minimum pinch radius of 2.1 mm at 150 ns and then goes out to 3.5 mm at 180 ns. Taking into account the time and distance error bars of the measured trajectory there is satisfactory agreement between the measured and computed trajectories especially in terms of the speeds. On close inspection of the comparison in Fig. 9, the measured minimum pinch radius appears to be significantly smaller than the computed. This features of divergence of computed from measured are the same as the case of UMDPF1, noted in Sec. IV of this paper.

VI. CONCLUSION

Comparison of the measured trajectory with the computed trajectory for the two machine shows features of agreement including general shape of the radial trajectory of the magnetic piston, and in the case of UMDPF1 also including the general shape of the radial shock trajectory. The average radial speed for the magnetic piston for each machine shows good agreement between the computed and

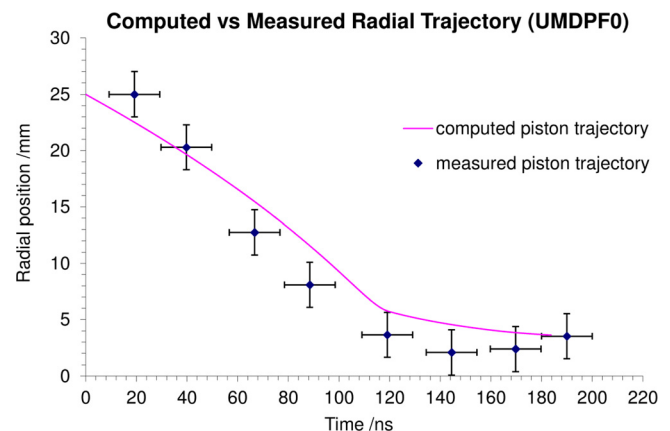FIG. 8. Computed and measured current waveform for UMDPF0 at pressure 0.3 Torr.

FIG. 9. Computed and measured radial trajectory of UMDPF0 in 0.3 Torr deuterium.

the measured values; this agreement is also shown by the average speed of the radial shock for UMDPF1. Thus, there is good agreement between the code and the measurements for the gross features of the dynamics for both machines. For both machines, there is good agreement for at least the first 80% of the radial trajectories with features of divergence only in the final stages of the compression.

For each machine, the measured minimum pinch radius is significantly smaller than the computed; for the UMDPF1, the measured minimum pinch radius ratio is 1.6 times smaller than the computed (0.09 measured versus 0.14 computed), whilst for the UMDPF0 the measured is 1.7 times smaller than the computed (0.08 measured versus 0.14 computed). Moreover, the final compression towards the minimum pinch radius is undoubtedly faster for each measured trajectory versus the computed trajectory in each machine. This indicates the limitation of the modelling during the pinch phase. The code considers the magnetic piston to remain as a clear-cut boundary between field-free plasma in front of the piston. However, in the actual situation this magnetic interface has slowed down considerably from the earlier high speed compression ($>10\,cm/\mu s$) to below $1\,cm/\mu s$ (in the last part of the compression) as can be seen from both Figs. 6 and 9. As a consequence, the magnetic Reynold's number (MRN) which depends on the speed of the magnetic interface to the power of four (4) would have dropped by a huge factor from much greater than 1 to much smaller than 1. From earlier work, for example, that presented in Ref. 46 for neon current sheets, we estimate that the transition speed from the regime of large MRN to small MRN for a deuterium current sheet is a few $cm/\mu s$. The consequence of this transition to slow MRN is that the magnetic field interface is no longer sharp towards the end of the compression, resulting in diffusion of magnetic field radially inwards into the previously relatively field-free plasma occurs. This would appear in framing and streak photographs as a further inward motion of the luminous front; leading to a measurement from plasma self-luminous images of a smaller radius than computed with our code which does not incorporate this mechanism of diffusion. It may also be noted that in the fitting of the current traces of each machine, the computed dip does not drop as low as the measured dip. This is consistent with the hypothesis of magnetic diffusion (towards the axis) which would increase the pinch inductance and cause a lower current dip than computed using a code that does not incorporate this mechanism of diffusion.

These results indicate that the Lee model code could be improved by the addition of this magnetic diffusion or an equivalent anomalous resistance mechanism into its computation of radial dynamics, particularly in the pinch phase. A start towards this has already been made[45] dealing with improving the fitting of the additional dip due to anomalous resistivity. However, this mechanism has not as yet been incorporated into the equations of motion of the code.

We discuss two important points inferred from the computed results for the UMDPFI. From the shock speed, the computed results give a temperature for the on-axis shock wave of 0.95×10^6 K and a reflected shock temperature of 2.2×10^6 K. The results also yield a peak pinch temperature of 4.6×10^6 K and a peak pinch density of 3.5×10^{24} ions m^{-3}. With these values of pinch temperature and density the observed neutron yield of the UMDPF1 of the order of 10^9 neutrons per shot could not be from thermalised plasma and is consistent with the neutron yield being from a beam-gas target mechanism. The second point relates to the axial shock speed arising from the radial compression processes. The code treats the plasma column as an elongating pinch; and the final elongation speed may be taken to be that of the post-pinch axial shock. The final pinch elongation speed is computed as $42\,cm/\mu s$ at the end of the pinch. In terms of application, the final pinch elongation speed may be compared with the post-pinch axial shock speed (of bubble) measured by Soto *et al.*[47] of $26\,cm/\mu s$ between $z = 9$ and $z = 16\,mm$ for the PF-400J. Soto *et al.* postulated that this observed axially moving "bubble" structure was a freely propagating strong shock wave with dramatically attenuating axial speed which dropped from average value of $26\,cm/\mu s$–$4.5\,cm/\mu s$ when measured between 9–16 mm and 16–20 mm, respectively. This would scale to a speed of $45\,cm/\mu s$ at the end of the pinch which is the start of the post-pinch axial shock propagation. We also ran the code configured as the PF-400J and obtained a final pinch elongation speed of $40.1\,cm/\mu s$. Thus, there is broad agreement that for a plasma focus of 400 J–6 kJ the axial shock at the end of the pinch is launched at a speed of around 40–$50\,cm/\mu s$. These plasma focus post-pinch axial shock waves are now considered as a useful tool for damage testing of fusion relevant wall-materials.[47,48]

In this paper, we have presented observed plasma focus radial trajectories and connected these observed results to computed end-of-pinch axial shock speeds which are currently of interest in experiments for damage on fusion relevant wall materials.

ACKNOWLEDGMENTS

[1]P. Kubes, M. Paduch, J. Cikhardt, D. Klir, J. Kravarik, K. Rezac, J. Kortanek, B. Cikhardtova, and E. Zielinska, "Existence of a return direction for plasma escaping from a pinched column in a plasma focus discharge," Phys. Plasmas **22**, 052706 (2015).

[2]M. Favre, P. Silva, P. Choi, H. Chuaqui, C. Dumitrescu-Zoita, and E. S. Wyndham, "Experimental investigations of hotspots in a low energy plasma focus operating in hydrogen-argon mixtures," IEEE Trans. Plasma Sci. **26**, 1154–1161 (1998).

[3]M. Z. Khan, S. L. Yap, Y. Ibrar, N. K. Nitturi, L. K. Lim, and C. S. Wong, "Low-energy plasma focus device as an electron beam source," Sci. World J. **2014**, 9 (2014).

[4]L. K. Lim, S. L. Yap, C. S. Wong, and M. Zakaullah, "Deuteron beam source based on Mather type plasma focus," J. Fusion Energy **32**, 287–292 (2013).

[5]S. K. Ngoi, S. L. Yap, C. S. Wong, and A. R. Saadah, "Ion beam measurements of a dense plasma focus device using CR 39 nuclear track detectors," AIP Conf. Proc. **1017**, 347–352 (2008).

[6]S. L. Yap, C. S. Wong, P. Choi, C. Dumitrescu, and S. P. Moo, "Observation of two phases of neutron emission in a low energy plasma focus," Jpn. J. Appl. Phys., Part 1 **44**, 8125–8132 (2005).

[7]H. R. Yousefi, S. R. Mohanty, Y. Nakada, H. Ito, and K. Masugata, "Compression and neutron and ion beams emission mechanisms within a plasma focus device," Phys. Plasmas **13**, 114506 (2006).

[8] D. E. Potter, "Numerical studies of the plasma focus," Phys. Fluids **14**, 1911–1924 (1971).

[9] T. Haruki, H. R. Yousefi, K. Masugata, J.-I. Sakai, Y. Mizuguchi, N. Makino, and H. Ito, "Simulation of high-energy particle production through sausage and kink instabilities in pinched plasma discharges," Phys. Plasmas **13**, 082106 (2006).

[10] F. Gratton and J. M. Vargas, "Two dimensional electromechanical model of the plasma focus," in *Energy Storage, Compression, and Switching*, edited by V. Nardi, H. Sahlin, and W. H. Bostick (Plenum, New York, 1983), **2**, 353.

[11] S. K. H. Auluck, "Bounds imposed on the sheath velocity of a dense plasma focus by conservation laws and ionization stability condition," Phys. Plasmas **21**, 090703 (2014).

[12] S. K. H. Auluck, "Global parameter optimization of a Mather-type plasma focus in the framework of the Gratton-Vargas two-dimensional snowplow model," Plasma Sources Sci. Technol. **23**, 065015 (2014).

[13] H. Jafari and M. Habibi, "Simulation of electrical discharge in a 3.6 joule miniature plasma focus device using SIMULINK," Eur. Phys. J. D **68**, 234 (2014).

[14] S. Lee, "Current and neutron scaling for megajoule plasma focus machines," Plasma Phys. Controlled Fusion **50**, 105005 (2008).

[15] S. Lee, "Plasma focus radiative model: Review of the Lee model code," J. Fusion Energy **33**, 1–17 (2014).

[16] S. Lee, "Radiative dense plasma focus computation package:RADPF," 2014.

[17] S. Lee and S. H. Saw, "Pinch current limitation effect in plasma focus," Appl. Phys. Lett. **92**, 021503 (2008).

[18] S. Lee, S. H. Saw, and J. Ali, "Numerical experiments on radiative cooling and collapse in plasma focus operated in krypton," J. Fusion Energy **32**, 42–49 (2013).

[19] D. E. Potter, "The formation of high-density z-pinches," Nucl. Fusion **18**, 813 (1978).

[20] M. Rosenbluth, "Dynamics of a pinched," in *Magnetohydrodynamics*, edited by R. Landshoff (Stanford University Press, Palo Alto, 1957), p. 57.

[21] M. Akel, S. A. Salo, S. H. Saw, and S. Lee, "Properties of ion beams generated by nitrogen plasma focus," J. Fusion Energy **33**, 189–197 (2014).

[22] S. Bing, "Plasma dynamics and X-ray emission of the plasma focus," Ph.D. thesis (Nanyang Technological University, Singapore, 2000).

[23] A. Jalil, "Development and studies of a small plasma focus," Ph.D. thesis (University of Malaya, Malaya, 1990).

[24] S. Lee, T. Y. Tou, S. P. Moo, M. A. Eissa, A. V. Gholap, K. H. Kwek, S. Mulyodrono, A. J. Smith, Suryadi, W. Usada, and M. Zakaullah, "A simple facility for the teaching of plasma dynamics and plasma nuclear fusion," Am. J. Phys. **56**, 62–68 (1988).

[25] M. Liu, "Soft X-rays from compact plasma focus," Ph.D. thesis (Nanyang Technological University, Singapore, 1996).

[26] S. H. Saw, P. C. K. Lee, R. S. Rawat, and S. Lee, "Optimizing UNU/ICTP PFF plasma focus for neon soft x-ray operation," IEEE Trans. Plasma Sci. **37**, 1276–1282 (2009).

[27] V. Siahpoush, M. A. Tafreshi, S. Sobhanian, and S. Khorram, "Adaptation of sing Lee's model to the Filippov type plasma focus geometry," Plasma Phys. Controlled Fusion **47**, 1065–1075 (2005).

[28] D. Wong, P. Lee, T. Zhang, A. Patran, T. L. Tan, R. S. Rawat, and S. Lee, "An improved radiative plasma focus model calibrated for neon-filled NX2 using a tapered anode," Plasma Sources Sci. Technol. **16**, 116–123 (2007).

[29] S. L. Yap, S. H. Lee, L. K. Lim, and C. S. Wong, "Dynamic studies of a small plasma focus device," In *Proceedings of the International Workshop On Plasma Computations & Applications (IWPCA2008), Kuala Lumpur, Malaysia* (2008), 51–54.

[30] S. Al-Hawat, "Axial velocity measurement of current sheath in a plasma focus device using a magnetic probe," IEEE Trans. Plasma Sci. **32**, 764–769 (2004).

[31] S. Lee, S. H. Saw, H. Hegazy, J. Ali, V. Damideh, N. Fatis, H. Kariri, A. Khabrani, and A. Mahasi, "Some generalised characteristics of the electrodynamics of the plasma focus in its axial phase: Illustrated by an application to independently determine the drive current fraction and the mass swept-up fraction," J. Fusion Energy **33**, 235–241 (2014).

[32] S. Lee and A. Serban, "Dimensions and lifetime of the plasma focus pinch," IEEE Trans. Plasma Sci. **24**, 1101–1105 (1996).

[33] S. H. Saw, M. Akel, P. C. K. Lee, S. T. Ong, S. N. Mohamad, F. D. Ismail, N. D. Nawi, K. Devi, R. M. Sabri, A. H. Baijan, J. Ali, and S. Lee, "Magnetic probe measurements in INTI plasma focus to determine dependence of axial speed with pressure in neon," J. Fusion Energy **31**, 411–417 (2012).

[34] T. Y. Tou, S. Lee, and K. H. Kwek, "Nonperturbing plasma-focus measurements in the run-down phase," IEEE Trans. Plasma Sci. **17**, 311–315 (1989).

[35] S. Zapryanov, V. Yordanov, and A. Blagoev, "On the current layer in the run-down phase of the plasma focus discharge," J. Phys.: Conf. Ser. **516**, 012029 (2014).

[36] A. Bernard, H. Bruzzone, P. Choi, H. Chuaqui, V. Gribkov, J. Herrera, K. Hirano, A. Krejci, S. Lee, C. Luo, F. Mezzetti, M. Sadowski, H. Schmidt, K. Ware, C. S. Wong, and V. Zoita, "Scientific status of plasma focus research," J. Moscow Phys. Soc. **8**, 93–170 (1998).

[37] M. Krishnan, "The dense plasma focus: A versatile dense pinch for diverse applications," IEEE Trans. Plasma Sci. **40**, 3189–3221 (2012).

[38] K. H. Kwek, "Pinch structure of a plasma focus," Ph.D. thesis (University of Malaya, Malaya, 1989).

[39] Y. H. Chen, "Study of coaxial plasma guns in mode operation," Ph.D. thesis (University of Malaya, Malaya, 1972).

[40] J. W. Mather, "Investigation of the high-energy acceleration mode in the coaxial gun," Phys. Fluids **7**, S28–S34 (1964).

[41] J. W. Shearer, "Contraction of z pinches actuated by radiation losses," Phys. Fluids **19**, 1426–1428 (1976).

[42] N. Khattak, "Anomalous heating (LHDI)," http://www.plasmafocus.net/IPFS/modelpackage/File3Appendix.pdf (2011).

[43] S. Lee, S. H. Saw, L. Soto, S. V. Springham, and S. P. Moo, "Numerical experiments on plasma focus neutron yield versus pressure compared with laboratory experiments," Plasma Phys. Controlled Fusion **51**, 075006 (2009).

[44] R. A. Behbahani and F. M. Aghamir, "Correlation of current drop, filling gas pressure, and ion beam emission in a low energy Mather-type plasma focus device," J. Appl. Phys. **111**, 043304 (2012).

[45] S. Lee, S. H. Saw, A. E. Abdou, and H. Torreblanca, "Characterizing plasma focus devices role of the static inductance instability phase fitted by anomalous resistances," J. Fusion Energy **30**, 277–282 (2011).

[46] S. H. Saw, S. H. Lee, P. C. K. Lee, R. S. Rawat, and K. Devi, "Magnetic Reynolds number and neon current sheet structure in the axial phase of a plasma focus," J. Fusion Energy **32**, 50–55 (2013).

[47] L. Soto, C. Pavez, J. Moreno, M. J. Inestrosa-Izurieta, F. Veloso, G. Gutirrez, J. Vergara, A. Clausse, H. Bruzzone, F. Castillo, and L. F. Delgado-Aparicio, "Characterization of the axial plasma shock in a table top plasma focus after the pinch and its possible application to testing materials for fusion reactors," Phys. Plasmas **21**, 122703 (2014).

[48] A. Cicuttin, M. Crespo, V. Gribkov, J. Niemela, C. Tuniz, C. Zanolli, M. Chernyshova, E. Demina, S. Latyshev, V. Pimenov, and A. Talab, "Experimental results on the irradiation of nuclear fusion relevant materials at the dense plasma focus Bora device," Nucl. Fusion **55**, 063037 (2015).